THE JOURNAL OF PHYSICAL CHEMISTRY B

ARTICLE

pubs.acs.org/JPCB

Solution-Based Structural Analysis of the Decaheme Cytochrome, MtrA, by Small-Angle X-ray Scattering and Analytical Ultracentrifugation

Mackenzie A. Firer-Sherwood,[†,∥] Nozomi Ando,[‡,§,∥] Catherine L. Drennan,[‡,§] and Sean J. Elliott*[,†]

[†]Department of Chemistry, Boston University, 590 Commonwealth Avenue, Boston, Massachusetts 02215, United States

[‡]Howard Hughes Medical Institute, [§]Departments of Biology and Chemistry, Massachusetts Institute of Technology, 77 Massachusetts Avenue, Cambridge, Massachusetts 02139, United States

Supporting Information

ABSTRACT: The potential exploitation of metal-reducing bacteria as a means for environmental cleanup or alternative fuel is an exciting prospect; however, the cellular processes that would allow for these applications need to be better understood. MtrA is a periplasmic decaheme *c*-type cytochrome from *Shewanella oneidensis* involved in the reduction of extracellular iron oxides and therefore is a critical element in *Shewanella* ability to engage in extracellular charge transfer. As a relatively small 333-residue protein, the heme content is surprisingly high. MtrA is believed to obtain electrons from the inner membrane-bound quinol oxidoreductase, CymA, and shuttle them across the outer membrane to MtrC, another decaheme cytochrome that directly interacts with insoluble metal oxides. How MtrA is able to perform this task is a question of interest. Here through the use of two solution-based techniques, small-angle X-ray scattering (SAXS) and analytical ultracentrifugation (AUC), we present the first structural analysis of MtrA. Our results establish that between 0.5 and 4 mg/mL, MtrA exists as a monomeric protein that is shaped like an extended molecular "wire" with a maximum protein dimension (D_{max}) of 104 Å and a rod-like aspect ratio of 2.2 to 2.5. This study contributes to a greater understanding of how MtrA fulfills its role in the redox processes that must occur before electrons reach the outside of the cell.

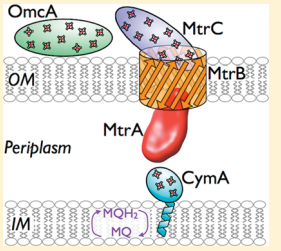

INTRODUCTION

The Gram negative bacterium *Shewanella oneidensis* belongs to a class of microorganisms that are capable of using a wide range of electron acceptors in the absence of oxygen, spanning organic compounds (e.g., fumarate)[1] to insoluble metal oxides[2,3] to soluble inorganic species such as uranyl and chromate ions.[4,5] In particular, its ability to couple external metal reduction to the oxidation of organic compounds via dissimilatory metal reduction (DMR) chemistry has made this bacterium a prominent candidate for application in bioremediation as well as microbial fuel cells.[3,6] Whereas *Shewanella* organisms appear to have degenerate pathways of electron transfer that enable growth by anaerobic DMR chemistry, several of the multiheme cytochromes of *Shewanella* encoded by the *mtr*CABDEF gene cluster have been shown to be responsible for its ability to make direct contact with metal oxides.[7−12] However, structural elucidation of any of the *Shewanella* cytochromes associated with the DMR pathway has proven to be elusive to date, aside from the characterization of OmcA by small-angle X-ray scattering (SAXS).[13] In this work, we have examined the size and shape of MtrA from *S. oneidensis*, a decaheme cytochrome that is proposed to provide an essential molecular "wire" that allows for passage of charge from the periplasm, across the outer membrane, to external electron acceptors.

In the current model of the DMR pathway schematized by Figure 1, MtrA is one of the multiple multiheme *c*-type cytochromes (which have heme cofactors covalently bound to the protein backbone through the cysteines found in the CXXCH heme-binding motif) that simultaneously generate a proton motive force across the cytoplasmic membrane, in part through the action of the tetraheme quinol oxidoreductase (CymA), and conduct charge across the periplasmic space and the outer membrane, ultimately to the cellular exterior by a series of decaheme proteins (MtrA, MtrC, and OmcA). Previously, we have used direct protein electrochemistry to demonstrate that electron transfer between these cytochromes is thermodynamically favorable,[14] existing as a chain of proteins by which long-range electron transfer occurs. These proteins shuttle electrons from the inside of the cell to the outside, where they directly reduce Fe(III) oxides.[10,15,16] CymA is postulated to be anchored to the cytoplasmic membrane by a single transmembrane helix and contain a globular head that inserts into the periplasmic space.[17,18] With this orientation, it is able to transfer electrons to many other redox partners such as MtrA. Recently, it has been proposed that MtrA and MtrC interact directly and are assembled into a MtrCAB complex, using the porin sheath of MtrB as a scaffold.[19] Finally, MtrC and OmcA are able to interact directly with and reduce extracellular Fe(III) oxides and have

Received: April 18, 2011
Revised: August 12, 2011
Published: August 12, 2011

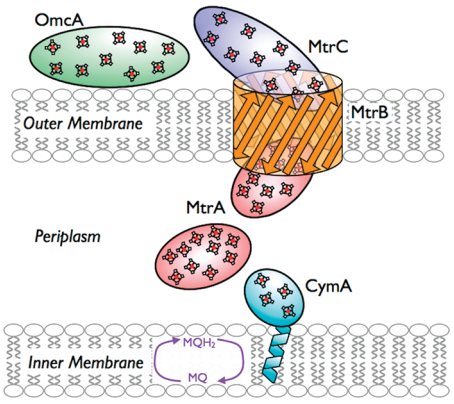

Figure 1. Proposed Fe(III) oxide electron transfer pathway in *Shewanella oneidensis* MR-1. MtrA is shown in two locations due to its potential dual functionality.

been shown to be localized to the outermembrane.[7,20−22] It has been suggested by Hartshorne and coworkers that the MtrCAB complex may represent a more widely used bioenergetic strategy for the electrical connection of the cellular periplasm with the exterior in a range of microbes capable of different bioenergetic pathways as orthologs can be found in *Shewanella* and other organisms.[19] Notably, in these cases, a decaheme protein similar to MtrA would serve as the critical electrical conduit to pass charge to reach the cellular surface. Currently, however, no high-resolution structures exist for the MtrCAB complex or any of its proposed substituents. Therefore, the molecular details of this DMR pathway generally and MtrA in particular remain poorly understood.

MtrA may perform a unique role in the electron transfer pathway as an intermediate periplasmic protein that is able to transport electrons from CymA to the outer membrane protein MtrC. With 333 amino acid residues and 10 low-spin heme cofactors proposed to possess *bis*-histidine coordination,[9] MtrA has a notably low amino acid to heme ratio of 33, whereas an average heme-bearing protein has approximately 60−70 amino acids per heme unit.[23] Crystal structures of other multiheme cytochromes have shown that the hemes are packed as a wire with edge-to-edge distances between 4 and 8 Å.[24,25] A similar packing of cofactors in MtrA would suggest that the protein is ∼100 Å long and thus able to span a substantial portion of the 130−250 Å distance across the periplasm.[26] In addition to shuttling electrons across the periplasm, MtrA is also thought to contact the outer membrane protein MtrC directly by docking in the MtrB porin protein. Such a function requires that at least one end of MtrA be narrow enough to fit in the MtrB porin barrel. In the absence of a crystal structure, the overall structure of MtrA has been hypothesized based on a sequence alignment with the structurally characterized NrfB, a pentaheme *c*-type cytochrome from *Escherichia coli* that purifies as a 40 kDa decaheme homodimer on a size exclusion column.[7,27] Sequence alignment of NrfB with the N-terminal half of MtrA shows alignment of the heme-binding motifs, leading to the hypothesis that MtrA forms two pentaheme modules with dimensions of an end-to-end NrfB homodimer: 80 Å in length and 30 Å, on average, in diameter.[12,28] These dimensions would presumably allow MtrA to insert partially into the MtrB porin. However, other than the heme-binding motifs of the N-terminal half of MtrA, the sequences of NrfB and MtrA show poor alignment, particularly along the C-terminal portion of the MtrA sequence. Therefore, it remains unknown if MtrA is structurally shaped like an electron "wire" and therefore able to perform both of its proposed functions.

Here we present the first structural characterization of MtrA from *S. oneidensis* using two complementary solution-based techniques: SAXS and analytical ultracentrifugation (AUC). Whereas AUC is particularly useful for probing the oligomerization state of proteins, SAXS is sensitive to electron density distributions with inhomogeneities on the length scales of 10 to 100 Å and thereby provides further structural detail of proteins in solution. Although SAXS does not provide high-resolution structural models, it is particularly useful for investigating proteins that are challenging to crystallize and has been successful in the characterization of the overall shape and length of spherical as well as elongated proteins.[29−32] Data from both techniques show that MtrA is monomeric over a wide range of protein concentrations and possesses a rod-like aspect ratio with a maximum dimension of 104 Å. This corroborates the previously proposed model of MtrA serving as a functional wire.[12,19] The data presented in this Article are a step toward understanding the structure of MtrA and how it shuttles electrons across the periplasmic space of *Shewanella*.

EXPERIMENTAL METHODS

Protein Expression and Purification. The plasmid containing *mtrA*, LS246, was provided by Dr. Liang Shi (Pacific Northwest National Laboratory). *E. coli* JM109(DE3) cells were transformed first with the pEC86 plasmid (provided by Linda Thöny-Meyer of ETH Zurich) containing the *ccm*ABCDEFG genes, then transformed with LS246. MtrA was expressed as previously described.[9] Cells were harvested at 8000*g* for 15 min at 4 °C. Lysis was completed through osmotic shock by resuspending the cell pellet in TES buffer (200 mM Tris-HCl, pH 8.0, 1 mM EDTA, and 500 mM sucrose) containing 1 mg/mL lysozyme and incubating on ice for 1 h. The lysed cells were spun at 18 000*g* for 30 min at 4 °C. Purification was carried out similarly to the published protocol,[9] with a few modifications. The supernatant was loaded onto DEAE resin, equilibrated with 10 mM Tris-HCl, pH 8.0 and MtrA was eluted using a linear gradient of 0−300 mM NaCl. Fractions containing MtrA were pooled and concentrated to ∼1 mL using a 10 kDa MWCO Amicon centrifugal device. This sample was loaded onto a HiPrep 26/60 Sephacryl S-100 high-resolution gel filtration column and eluted with 20 mM HEPES, pH 8.0, 50 mM NaCl using a GE AKTA FPLC system. Fractions were tested for purity using SDS-PAGE and UV−vis absorbance; those displaying a single band and a purity index (A_{409}/A_{280}) greater than 2.0 were pooled and concentrated for a final purity index of 2.8.

Analytical Ultracentrifugation. Sedimentation velocity AUC was performed using a Beckman XL-I analytical ultracentrifuge (Beckman Coulter, Brea, CA) at the MIT Biophysical Instrumentation Facility. Fresh samples of 0.5 mg/mL MtrA were dialyzed against 20 mM HEPES, pH 8.0, 50 mM NaCl. The protein solution and dialysate were loaded into two-sector cells and equilibrated for 10 h to reach a temperature of 20.0 °C prior to centrifugation at a rotor speed of 40 000 rpm. The protein concentration across the cell was measured by monitoring the heme absorbance at 420 nm at 2 min intervals.

The apparent sedimentation coefficient distribution, $g(s^*)$, was generated from 42 scans with a peak broadening limit of 180 kDa

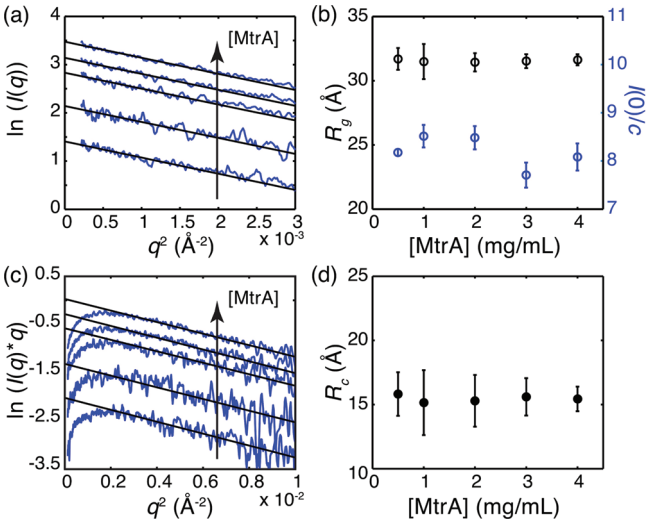

Figure 2. Overall and cross-sectional size of 0.5, 1, 2, 3, and 4 mg/mL MtrA studied by SAXS. (a) Guinier plots show good linearity at low q, indicating a lack of nonspecific aggregation. The radius of gyration, R_g, and normalized zero-angle scattering intensity $I(0)/c$ were determined from linear fits (black) to the data (blue), where the Guinier approximation (eq 1) holds. (b) R_g and $I(0)/c$ are concentration-independent, suggesting that the oligomerization state does not change under these conditions. (c) Cross-sectional Guinier plots display linear regions, indicative of elongated shape of MtrA. The cross-sectional radius of gyration R_c was determined from linear fits (black) to the data (blue), where eq 2 holds. (d) R_c is also concentration-independent. Protein concentration increases from bottom to top in (a) and (c).

using the dc/dt method implemented in the program DCDT+.[33] The diffusion-deconvoluted sedimentation coefficient distribution, $c(s)$, was generated from 280 scans in the program SedFit.[34] The sedimentation coefficients were converted to standard values ($s_{20,w}$) using a solvent viscosity and density of 1.0221×10^{-2} poise and 1.00185 g/mL (calculated in Sednterp[35]), respectively. The average partial specific volume of proteins, 0.73 mL/g,[36] was used for this conversion, as the heme contribution to this quantity cannot be easily determined. The molecular weight of monomeric MtrA with 10 hemes was calculated to be 42.8 kDa.

Small-Angle X-ray Scattering. SAXS was performed at the Cornell High Energy Synchrotron Source G1 station (CHESS, Cornell University, Ithaca, NY) using a 10.5 keV 250 μm square X-ray beam with a flux of several 10^{12} photons/s. Data were collected at room temperature on a 1024 × 1024 pixel CCD detector similar to that described in ref 37 at a sample-to-detector distance of 1 m; the transmission intensity was measured with a PIN diode beamstop.

Protein solution scattering was measured from fresh samples of 0.5, 1, 2, 3, and 4 mg/mL MtrA in 20 mM HEPES, pH 8.0, 50 mM NaCl contained in acrylic laminate static cells with 7.5 μm thick polyimide film windows.[38] Background scattering was measured with buffer in the same cells. Detailed data acquisition and reduction procedures are described by Ando et al.[38] Transmission-normalized background subtraction yielded the scattering profiles, scattering intensity (I) versus momentum transfer (q); here $q = 4\pi/\lambda \sin\theta$, where λ is the X-ray wavelength and 2θ is the scattering angle with respect to the X-ray beam. The foldedness of MtrA under the investigated conditions was verified by Kratky analysis; a representative plot is shown in Figure S1 of the Supporting Information.

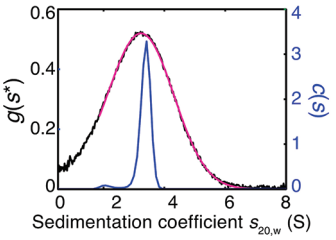

Figure 3. Molecular weight determination of 0.5 mg/mL MtrA by sedimentation velocity AUC. The apparent sedimentation coefficient distributions $g(s^*)$ fit with single Gaussian, black and magenta curves, respectively, and the diffusion-deconvoluted sedimentation coefficient distribution $c(s)$, blue curve, indicate that MtrA is monomeric.

The zero-angle scattering intensity $I(0)$ and overall radius of gyration R_g were obtained from a Guinier approximation to the low-q region of the scattering profiles satisfying the condition, $q^*R_g < 1.3$.[39]

$$I(q) \approx I(0) \exp(-R_g^2 q^2/3) \quad (1)$$

In the case of elongated proteins, a cross-sectional radius of gyration, R_c, can be determined using a similar approximation as in eq 1.[39]

$$I(q)*q \approx I(0) \exp(-R_c^2 q^2/2) \quad (2)$$

R_g and $I(0)$ are determined from linear fits to Guinier plots, $\ln(I(q))$ versus q^2. Likewise, R_c is determined from cross-sectional Guinier plots, $\ln(I(q)*q)$ versus q^2.

RESULTS

The size and concentration dependence of MtrA were investigated by SAXS over a concentration range of 0.5−4 mg/mL. Guinier analysis was used to determined the overall radius of gyration, R_g, and the concentration-normalized forward scattering intensity, $I(0)/c$, which are functions of spatial size and molecular mass, respectively.[40] The Guinier plots are linear at the low q-range displayed in Figure 2a at all concentrations, indicating that MtrA has a well-defined size under the solution conditions studied and that radiation-induced aggregation is not an issue. R_g and $I(0)/c$, determined from linear fits to the data over the q range satisfying the $q^*R_g < 1.3$ condition (q = 0.0146 to 0.0416 Å^{-1}), display very little concentration dependence (Figure 2b), indicating that no change in oligomerization state occurs over the investigated concentration range.

The oligomerization state of MtrA was determined by sedimentation velocity AUC at one of the protein concentrations investigated by SAXS under identical solution conditions. A single peak is observed in $g(s^*)$ that is well-described by a single Gaussian over the range $s_{20,w}$ = 2 − 7 S, indicative of a single dominant species under nearly ideal conditions (black and magenta curves in Figure 3).[41] The slight peak broadening in $g(s^*)$ at $s_{20,w} < 2$ S is consistent with the observation of a small peak in $c(s)$ (blue curve in Figure 3) and can be attributed to proteolysis (unpublished data). The molecular weight and $s_{20,w}$ of the dominant species were determined to be 35.6 kDa and 3.4 S by the Svedberg relation in DCDT+. Similar values of 36.9 kDa and 3.4 S were determined from $c(s)$ in SedFit, most consistent with that of a 42.8 kDa monomeric state.

The shape of the MtrA monomer was analyzed by SAXS. Using the indirect Fourier transform method implemented in the

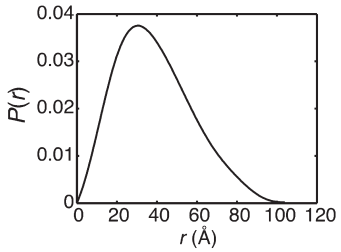

Figure 4. Pair distance distribution, $P(r)$, determined from SAXS data collected on 3 mg/mL MtrA. The maximum dimension, D_{max}, is 104 Å, whereas the peak position lies at less than $D_{max}/2$, suggesting that MtrA is elongated.

program GNOM,[42] $I(q)$ of 3 mg/mL MtrA (over the range $q = 0.0174$ to 0.2047 Å^{-1}) was converted to a real space function, the pair distance distribution $P(r)$ with a reasonable total GNOM estimate of 0.619 (Figure 4).[43] $P(r)$ approaches zero as r approached a value of 104 Å for the maximum chord length, D_{max}. The skewed shape of $P(r)$, with a maximum at less than $D_{max}/2$, suggests that the MtrA monomer is an elongated species. Consistent with an elongated shape, the scattering curves plotted as cross-sectional Guinier plots, $\ln(I(q)^*q)$ versus q^2 (Figure 2c), display linear regions. In this representation, the length factor $(1/q)$ is removed, providing information on the cross-sectional size. Linear fits over the range $q = 0.069$ to 0.086 Å^{-1}, satisfying the $q^*R_c < 1.3$ condition, yielded the cross-sectional radius of gyration, R_c (Figure 2d). Excluded volume and other interparticle effects were removed from R_g and R_c by linear extrapolations of the values determined at 0.5 to 4 mg/mL to zero protein concentration, yielding values of 31.6 (±0.4) and 15.5 (±0.8) Å, respectively.

To visualize the overall shape of MtrA, we performed ab initio shape reconstructions on SAXS data collected at 3 mg/mL. Twenty bead models were generated with the simulated annealing program dammif 1.1.0,[44] all with reasonable goodness-of-fit to the original data ($\chi^2 = 3.89$). A comparison of the original SAXS data and the calculated scattering from a typical model is shown in Figure 5a. The calculated scattering of the model fits the experimental scattering particularly well at $q < 0.1$ Å^{-1}, where the overall shape information is stored. The apparent discrepancy between the model and experimental data in the high-q region can be attributed to a constant background subtraction implemented in dammif to impose a q^{-4} decay in the Porod region;[45] whereas this difference appears significant on a log scale, it is only 0.168 on a linear scale in scattering intensity, or 0.7% of $I(0)$ and is within the errors of background subtraction. Eighteen bead models were chosen by the alignment and averaging program damaver[46] with a normalized spatial discrepancy (NSD) of 0.662 ($\sigma^2 = 0.047$) to produce the final averaged model (Figure 5b). The average shape reconstructed by dammif is elongated in one dimension: ~100 Å in length, consistent with D_{max}, and approximately 25 Å × 50 Å at the largest cross section.

Because MtrA contains both heavy atoms (10 irons) and light atoms (protein and heme rings), we considered whether the usage of uniform-density beads by DAMMIF could affect shape reconstructions, despite minimizing the iron scattering contributions by the use of nonresonant X-ray energy for data collection. Using the program CRYSOL[47] and the crystal structure of the pentaheme NrfB, we found that irons contribute more to the overall intensity rather than the shape of the scattering curve,

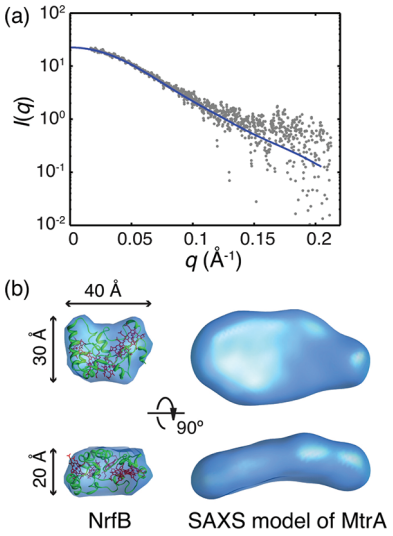

Figure 5. Ab initio shape reconstructions from SAXS data collected on 3 mg/mL MtrA. (a) SAXS data (gray dots) are shown with the calculated scattering of a representative model reconstructed by dammif.[44] (b) Molecular surface of the averaged shape reconstructed by dammif[44] compared with the NrfB surface smoothed to 15 Å resolution in Chimera.[59]

particularly at low resolution. Removal of the irons or entire hemes from the NrfB crystal structure leads to 0.2 to 0.3 Å changes in the calculated R_g, with very little change in the shape of the scattering curves up to $q = 0.2$ Å^{-1}. Such small changes in shape and size are within experimental error and thus are unlikely to affect the shape reconstructions presented here significantly.

DISCUSSION

MtrA is believed to be an essential component in the electron transfer pathway that allows *Shewanella oneidensis* to interact directly with iron oxides.[9,12,15] As one of the few known periplasmic proteins in this electron transfer chain, it likely carries out a critical step in shuttling electrons from the tetraheme cytochrome, CymA, to the outer membrane cytochromes that reduce iron oxide. Here we present the first solution-based structural analysis of MtrA using two complementary techniques, SAXS and AUC. Our AUC data indicate that at 0.5 mg/mL MtrA exists as a monomer. The monomeric state of MtrA is supported by our SAXS data, which show that there is no change in size when the concentration of protein is increased to 4 mg/mL. The pair distance distribution $P(r)$ determined by SAXS data suggests that MtrA is elongated in one dimension with a D_{max} of 104 Å. It is noted that D_{max} is sensitive to the quality of scattering data at low q, where parasitic scattering, interparticle effects, as well as effects of radiation damage dominate.[48] Therefore, it is important that D_{max} determined in this way be interpreted as an approximate quantity. However, the smooth decrease in $P(r)$ to D_{max} suggests that the elongated shape of MtrA is due to its inherent shape rather than due to aggregation. We also considered the effect of heme irons on SAXS data analysis using the structure of NrfB as a guide. Calculations suggest that changes to protein scattering curves due to the presence of bound iron atoms are within the experimental error, especially at the X-ray energy used here. Whereas it is outside the scope of this study, it is interesting to consider the use of anomalous iron scattering to characterize heme spatial distributions in multiheme proteins.[49]

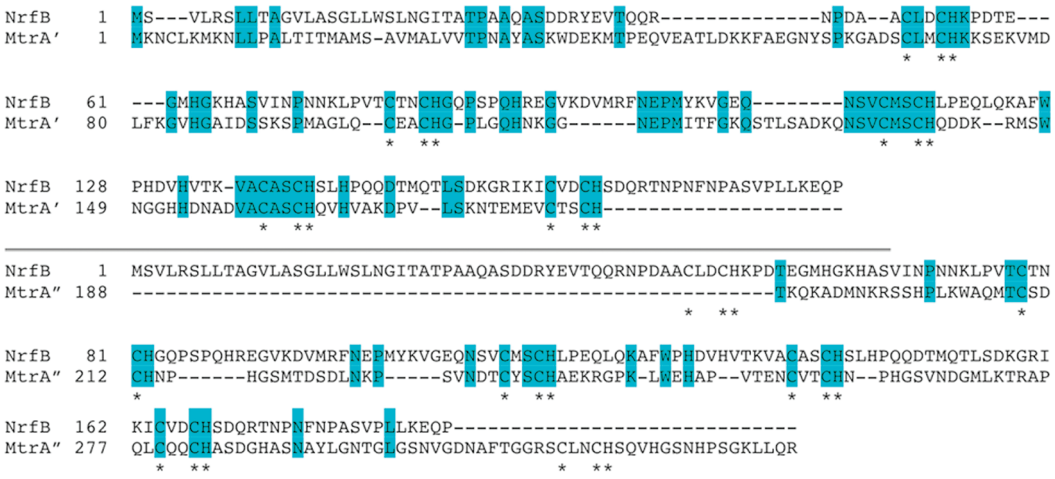

Figure 6. Sequence alignment of NrfB with N-terminal sequence of MtrA, MtrA′ (top), and C-terminal sequence of MtrA, MtrA′′ (bottom). Identical residues are shaded with blue, and the CXXCH motifs are indicated with asterisks.

Using SAXS data, the dummy residue model for MtrA determined by ab initio shape reconstructions is at least two times longer in one dimension than the perpendicular axes (Figure 5b). This aspect ratio of MtrA can be checked by a simple geometric calculation using the R_g and R_c values extrapolated to zero protein concentration. For a prolate ellipsoid of uniform density with a length $2c$ and cross-sectional semiaxes a and b,

$$R_g^2 = (a^2 + b^2 + c^2)/5 = R_c^2 + c^2/5 \quad (3)$$

Approximating the cross section as circular, that is, $a = b$, substitution of the experimental R_g and R_c gives semiaxes of 24.5 and 61.6 Å with an axial ratio of 2.5. As this axial ratio is >1, that of a sphere, MtrA must be elongated along one dimension, consistent with $P(r)$ and the ab initio shape reconstructions. This axial ratio is also in reasonable agreement with that obtained by sedimentation velocity AUC. Modeling MtrA as a prolate ellipsoid in SedFit yielded an axial ratio of 2.2 from the fitted hydrodynamic frictional ratio. Additionally, the theoretical $s_{20,w}$ of the SAXS model was calculated with SOMO[50] for comparison with the value determined experimentally by AUC. Using a partial specific volume of 0.73 mL/g (the average value for proteins[36]) and the molecular weight for a monomeric MtrA, the theoretical $s_{20,w}$ was calculated to be 3.1 S, in reasonable agreement with the experimental value of 3.4 S. Together, these results support the overall shapes of the reconstructed models that are up to 104 Å in length and up to 50 Å in the widest cross-sectional dimension.

Previously, it has been proposed that MtrA may be similar in shape to an end-to-end repeat of the pentaheme protein NrfB.[12] The shape reconstructions presented here suggest that the cross section of MtrA is elliptical rather than spherical, similar to the pentaheme NrfB from *E. coli*, and does appear somewhat evocative of a repeat of the NrfB fold (Figure 5b), where NrfB has dimensions of 40 Å × 30 Å × 20 Å in its crystal structure (Figure 5b).[28] However, the sequence alignments suggest that the potential relationship between NrfB and MtrA should only be taken so far: whereas the five CXXCH motifs in the N-terminal domain of MtrA (MtrA′) can be aligned with those in NrfB (NCBI BLAST[51]), giving an E value of 1×10^{-15} (Figure 6, top), the two halves of MtrA do not align particularly well with one another (E value is 1×10^{-4}), and the C-terminal domain of MtrA (MtrA′′) aligns with NrfB quite poorly, yielding an E value of only 0.007 (Figure 6, bottom). Moreover, whereas one molecule of NrfB will fit within the SAXS-derived surface reconstruction of MtrA, it is not possible to model two end-to-end NrfB monomers such that the pentaheme modules are within electron transfer distance without imposing arbitrary changes to the structural scaffold. Therefore, it is unclear if the entirety of MtrA could be reasonably modeled as being composed of two NrfB modules, in terms of key details such as the stacking of heme cofactors. We do note that repetition of multiheme motifs is not unprecedented among *c*-type cytochromes because sequence analysis of the dodecaheme cytochrome from *Geobacter sulfurreducens* shows that it consists of four triheme domains that align with the triheme cytochrome c_7.[52,53] Regardless of applicability of NrfB as a structural model for the entirety of MtrA, our data provide the first structural evidence that MtrA is indeed elongated like a wire.

With this information in hand, we can consider two of the proposed roles for MtrA: receiving electrons from inner membrane-bound CymA and directing them across the periplasm to the outer membrane, and shuttling electrons through the outer membrane to MtrC via the β-barrel porin protein MtrB (Figure 1).[19] First, we can now build upon our previous result that MtrA can directly accept electrons from the inner-membrane bound quinol oxidoreductase CymA,[19,54] and we can estimate that one ∼100 Å long MtrA molecule contacting CymA could span much of the 130−250 Å distance of periplasmic space.[26] Without knowing to what degree CymA or MtrB are extended into the periplasm and with such a large uncertainty in the periplasmic distance, we cannot predict how far a single MtrA molecule would need to travel or if it would need to travel at all to engage in redox shuttling. We can say that in the absence of a stabilizing factor, it is unlikely that end-to-end MtrA molecules are involved in this process because our data show that MtrA alone does not oligomerize up to protein concentrations of 4 mg/mL.

The second proposed function for MtrA is that it could pass electrons directly to the outer membrane cytochrome MtrC when both are docked within the MtrB β-barrel. (See Figure 1.) Whereas the structure of MtrB is unknown, it is predicted to be a 28-strand β-barrel protein using the PRED-TMBB prediction program.[55,56] The size of a transmembrane β-barrel can be

estimated by sequence and is dependent on the number of strands, n, and shear number, S,[57] a numerical parameter corresponding to the pitch of the β-barrel. Shear numbers range between n and $n + 4$ with a few exceptions,[57] and pore size will increase with larger values of n and S.[57] A slightly smaller β-barrel protein, FepA, has 22 strands with a shear number of +24, and its crystal structure gives an elliptical pore size of 30 Å × 40 Å.[58] Therefore, presuming that MtrB is a subparallel β-barrel as predicted, it is reasonable to think of MtrB with slightly larger pore dimensions than FepA. In this light, the dimensions of MtrA estimated by SAXS (approximately 25 Å × 50 Å at the largest cross-section by 104 Å in length) are provocative, suggesting that MtrA would at least be able to insert partially into the β-barrel MtrB, if not span the entire outer membrane. The electron recipient, MtrC, has not been structurally characterized but is 43% similar to OmcA (E value of 7×10^{-18}), which has been estimated by SAXS to have dimensions that are wider and shorter than MtrA (34 Å × 65 Å × 90 Å for OmcA) but still are of a range that could fit partially into the MtrB barrel structure.[13]

CONCLUSIONS

The combined use of AUC and SAXS has enabled us to characterize the structure of MtrA in solution for the first time. We have demonstrated that at all concentrations studied, MtrA exists as an extended monomer with a maximum dimension of 104 Å with an aspect ratio of 2.5 when modeled as a prolate ellipsoid. This is the first biophysical evidence that supports the proposed physiological functions of MtrA as a periplasmic electron shuttle. The dimensions and shape indicate that it is possible for MtrA to accept electrons from CymA and then donate them to MtrC via the MtrB β-barrel.[19,54] As it has been suggested that decaheme orthologs for MtrA may represent a novel, yet wide-ranging strategy for extracellular redox communication in anaerobic micro-organisms,[19] our data represent the latest, key step toward a unified view of multiheme cytochromes as components of long-distance "wires" in nature.

ASSOCIATED CONTENT

Supporting Information. Kratky analysis of MtrA SAXS data. This material is available free of charge via the Internet at http://pubs.acs.org.

AUTHOR INFORMATION

Corresponding Author

*Tel: 617-358-2816. Fax: 617-353-6466. E-mail: elliott@bu.edu.

Author Contributions

‖These authors contributed equally to this publication.

ACKNOWLEDGMENT

This work was generously supported by the NSF (S.J.E., MCB 0546323) and NIH grant F32GM904862 (N.A.). C.L.D. is a Howard Hughes Medical Institute Investigator. CHESS is supported by the NSF & NIH/NIGMS via NSF award DMR-0936384. We thank Liang Shi (PNNL) for the donation of the MtrA plasmid, Linda Thöny-Meyer (ETH Zurich) for the donation of the pEC86 vector, Arthur Woll (CHESS) for assistance with SAXS experimental setup, Debbie Pheasant (MIT BIF) for assistance with AUC data collection, Emre Brookes and Borries Demeler (UT Health Science Center) for assistance with SOMO, Cynthia Kinsland for use of the Cornell Protein Facility, and Rebekah Bjork (MIT) for assistance with SAXS data collection. Molecular graphics images were produced using the UCSF Chimera package from the Resource for Biocomputing, Visualization, and Informatics at the University of California, San Francisco (supported by NIH P41 RR001081).

REFERENCES

(1) Myers, C. R.; Nealson, K. H. *Science* **1988**, *240*, 319–321.
(2) Myers, C. R.; Nealson, K. H. *J. Bacteriol.* **1990**, *172*, 6232–6238.
(3) Lovley, D. R. *Microbiol. Rev.* **1991**, *55*, 259–287.
(4) Lovley, D. R.; Phillips, E. J. P.; Gorby, Y. A.; Landa, E. R. *Nature* **1991**, *350*, 413–416.
(5) Myers, C. R.; Carstens, B. P.; Antholine, W. E.; Myers, J. M. *J. Appl. Microbiol.* **2000**, *88*, 98–106.
(6) Lovley, D. R. *Annu. Rev. Microbiol.* **1993**, *47*, 263–290.
(7) Beliaev, A. S.; Saffarini, D. *J. Bacteriol.* **1998**, *180*, 6292–6297.
(8) Beliaev, A. S.; Saffarini, D.; McLaughlin, J. L.; Hunnicutt, D. *Mol. Microbiol.* **2001**, *39*, 722–730.
(9) Pitts, K. E.; Dobbin, P. S.; Reyes-Ramirez, F.; Thomson, A. J.; Richardson, D. J.; Seward, H. E. *J. Biol. Chem.* **2003**, *278*, 27758–27765.
(10) Xiong, Y.; Shi, L.; Baowei, C.; Mayer, M. U.; Lower, B. H.; Londer, Y. Y.; Bose, S.; Hochella, M. F.; Fredrickson, J. K.; Squier, T. C. *J. Am. Chem. Soc.* **2006**, *128*, 13978–13979.
(11) Shi, L.; Squire, T. C.; Zachara, J.; Fredrickson, J. *Mol. Microbiol.* **2007**, *65*, 12–20.
(12) Clarke, T. A.; Holley, T.; Hartshorne, R. S.; Fredrickson, J. K.; Zachara, J. M.; Shi, L.; Richardson, D. J. *Biochem. Soc. Trans.* **2008**, *36*, 1005–1010.
(13) Johs, A.; Shi, L.; Droubay, T.; Ankner, J. F.; Liang, L. *Biophys. J.* **2010**, *98*, 3035–3043.
(14) Firer-Sherwood, M. A; Pulcu, G. S.; Elliott, S. J. *J. Biol. Inorg. Chem.* **2008**, *13*, 849–854.
(15) Hartshorne, R. S.; Jepson, B. N.; Clarke, T. A.; Field, S. J.; Fredrickson, J.; Zachara, J.; Shi, L.; Butt, J. N.; Richardson, D. J. *J. Biol. Inorg. Chem.* **2007**, *12*, 1083–1094.
(16) Lower, B. H; Shi, L.; Yongsunthon, R.; Droubay, T. C.; McCready, D. E.; Lower, S. K. *J. Bacteriol.* **2007**, *189*, 4944–4952.
(17) Myers, C. R.; Myers, J. M. *J. Bacteriol.* **1997**, *179*, 1143–1152.
(18) Schwalb, C.; Chapman, S. K.; Reid, G. A. *Biochem. Soc. Trans.* **2002**, *30*, 658–662.
(19) Hartshorne, R. S.; Reardon, C. L.; Ross, D.; Nuester, J.; Clarke, T. A.; Gates, A. J.; Mills, P. C.; Fredrickson, J. K.; Zarchara, J. M.; Shi, L.; Beliaev, A. S.; Marshall, M. J.; Tien, M.; Brantley, S.; Butt, J. N.; Richardson, D. J. *Proc. Natl. Acad. Sci. U.S.A.* **2009**, *106*, 22169–22174.
(20) Lower, B. H.; Yongsunthon, R.; Shi, L.; Wildling, L.; Gruber, H. J.; Wigginton, N. S.; Reardon, C. L.; Pinchuk, G. E.; Droubay, T. C.; Boily, J.-F.; Lower, S. K. *Appl. Environ. Microbiol.* **2009**, *75*, 2931–2935.
(21) Donald, J. W.; Hicks, M. G.; Richardson, D. J.; Palmer, T. *J. Bacteriol.* **2008**, *190*, 5127–5131.
(22) Shi, L.; Chen, B.; Wang, Z.; Elias, D. A.; Mayer, M. U.; Gorby, Y. A. *J. Bacteriol.* **2006**, *188*, 4705–4714.
(23) Sharma, S.; Cavallaro, G.; Rosato, A. *J. Biol. Inorg. Chem.* **2010**, *15*, 559–571.
(24) Taylor, P.; Pealing, S. L.; Reid, G. A.; Chapman, S. K.; Walkinshaw, M. D. *Nat. Struct. Biol.* **1999**, *6*, 1108–1112.
(25) Igarashi, N.; Moriyama, H.; Fujiwara, T.; Fukumori, Y.; Tanaka, N. *Nat. Struct. Biol.* **1997**, *4*, 276–284.
(26) Seltmann, G., Holst, O. Periplasmic Space and Rigid Layer. Periplasmic Space and Rigid Layer. In *The Bacterial Cell Wall*; Springer: New York, 2002; pp 103−128.
(27) Clarke, T. A.; Dennison, V.; Seward, H. E.; Burlat, B.; Cole, J. A.; Hemmings, A. M.; Richardson, D. J. *J. Biol. Chem.* **2004**, *279*, 41333–41339.

(28) Clarke, T. A.; Cole, J. A.; Richardson, D. J.; Hemmings, A. M. *Biochem. J.* **2007**, *406*, 19–30.
(29) Pinotsis, N.; Lange, S.; Perriard, J. C.; Svergun, D. I.; Wilmanns, M. *EMBO J.* **2008**, *27*, 253–264.
(30) Tanaka, Y.; Sakamoto, S.; Kuroda, M.; Goda, S.; Gao, Y.-G.; Tsumoto, K.; Hiragi, Y.; Yao, M.; Watanabe, N.; Ohta, T.; Tanaka, I. *Structure* **2008**, *16*, 488–496.
(31) Sokolova, A. V.; Volkov, V. V.; Svergun, D. I. *Crystallogr. Rep.* **2003**, *48*, 959–965.
(32) Putnam, C. D.; Hammel, M.; Hura, G. L.; Tainer, J. A. *Q. Rev. Biophys.* **2007**, *40*, 191–285.
(33) Philo, J. S. *Anal. Biochem.* **2006**, *354*, 238–246.
(34) Brown, P. H.; Schuck, P. *Biophys. J.* **2006**, *90*, 4651–4661.
(35) Laue, T. M.; Shah, B. D.; Ridgeway, T. M.; Pelletier, S. L. *Analytical Ultracentrifugation in Biochemistry and Polymer Science*; Harding, S. E., Horton, J. C., Eds.; The Royal Society of Chemistry: Cambridge, U.K., 1992; pp 90−125.
(36) Quillin, M. L.; Matthews, B. W. *Acta Crystallogr., Sect. D: Biol. Crystallogr.* **2000**, *56*, 791–794.
(37) Tate, M. W.; Eikenberry, E. F.; Barna, S. L.; Wall, M. E.; Lowrance, J. L.; Gruner, S. M. *J. Appl. Crystallogr.* **1995**, *28*, 196–205.
(38) Ando, N.; Chenevier, P.; Novak, M.; Tate, M. W.; Gruner, S. M. *J. Appl. Crystallogr.* **2008**, *41*, 167–175.
(39) Svergun, D. I.; Koch, M. H. J. *Rep. Prog. Phys.* **2003**, *66*, 1735.
(40) Glatter, O., Kratky, O. *Small Angle X-ray Scattering*; Academic Press: London, 1982; pp 1−515.
(41) Philo, J. S. *Anal. Biochem.* **2000**, *279*, 151–163.
(42) Konarev, P. V.; Volkov, V. V.; Sokolova, A. V.; Koch, M. H. J.; Svergun, D. I. *J. Appl. Crystallogr.* **2003**, *36*, 1277–1282.
(43) Svergun, D. I. *J. Appl. Crystallogr.* **1992**, *25*, 495–503.
(44) Franke, D.; Svergun, D. I. *J. Appl. Crystallogr.* **2009**, *42*, 342–346.
(45) Svergun, D. I. *Biophys. J.* **1999**, *76*, 2879–2886.
(46) Volkov, V. V.; Svergun, D. I. *J. Appl. Crystallogr.* **2003**, *36*, 860–864.
(47) Svergun, D. I.; Barberato, C.; Koch, M. H. J. *J. Appl. Crystallogr.* **1995**, *28*, 768–773.
(48) Jacques, D. A.; Trewhella, J. *Protein Sci.* **2010**, *19*, 642–657.
(49) Feigin, L. A., Svergun, D. I. *Structural Analysis by Small-Angle X-Ray and Neutron Scattering*; Plenum Press: New York, 1987; pp 1−335.
(50) Brookes, E.; Demeler, B.; Rosano, C.; Rocco, M. *Eur. Biophys. J.* **2010**, *39*, 423–435.
(51) Altschul, S. F.; Madden, T. F.; Schaffer, A. A.; Zhang, J.; Zhang, Z.; Miller, W.; Lipman, D. J. *Nucleic Acids Res.* **1997**, *25*, 2289–3402.
(52) Pokkuluri, P. R.; Londer, Y. Y.; Duke, N. E. C.; Erickson, J.; Pessanha, M.; Salgueiro, C. A.; Schiffer, M. *Protein Sci.* **2004**, *13*, 1684–1692.
(53) Londer, Y. Y.; Pokkuluri, P. R.; Erickson, J.; Orshonsky, V.; Schiffer, M. *Protein Expression Purif.* **2005**, *39*, 254–260.
(54) Firer-Sherwood, M. A.; Bewley, K. D.; Mock, J. Y.; Elliott, S. J. *Metallomics* **2011**, *3*, 344–348.
(55) Bagos, P. G.; Liakopoulous, T. D.; Spyropoulos, I. C.; Hamodrakas, S. J. *BMC Bioinf.* **2004**, *5*, 29–42.
(56) Bagos, P. G.; Liakopoulous, T. D.; Spyropoulos, I. C.; Hamodrakas, S. J. *Nucleic Acids Res.* **2004**, *32*, 400–404.
(57) Schulz, G. E. *Biochim. Biophys. Acta* **2002**, *1565*, 308–317.
(58) Buchanan, S. K.; Smith, B. S.; Venkatramani, L.; Xia, D.; Esser, L.; Palnitkar, M.; Chakraborty, R.; van der Helm, D.; Deisenhofer, J. *Nat. Struct. Biol.* **1999**, *6*, 56–63.
(59) Pettersen, E. F.; Goddard, T. D.; Huang, C. C.; Couch, G. S.; Greenblatt, D. M.; Meng, E. C.; Ferrin, T. E. *J. Comput. Chem.* **2004**, *25*, 1605–1612.